Solitons in a nonlinear Schrödinger equation with $\mathcal{PT}$-symmetric potentials and inhomogeneous nonlinearity: Stability and excitation of nonlinear modes

Zhenya Yan,[1,*] Zichao Wen,[1] and Vladimir V. Konotop[2]

[1]*Key Laboratory of Mathematics Mechanization, Institute of Systems Science, AMSS, Chinese Academy of Sciences, Beijing 100190, China*

[2]*Centro de Física Teórica e Computacional and Departamento de Física, Faculdade de Ciências, Universidade de Lisboa, Campo Grande, Edifício C8, Lisboa 1749-016, Portugal*

(Received 16 May 2015; published 13 August 2015)

We report branches of explicit expressions for nonlinear modes in parity-time ($\mathcal{PT}$)-symmetric potentials of several types. For the single-well and double-well potentials the found solutions are two-parametric and appear to be stable even when the $\mathcal{PT}$ symmetry of respective underlying linear models is broken. Based on the examples of these solutions we describe an algorithm of excitation of a stable nonlinear mode in a model whose linear limit is unstable. The method is based on the adiabatic change of the control parameter driving the mode along a branch bifurcating from a stable linear mode. The suggested algorithm is confirmed by extensive numerical simulations.

DOI: 10.1103/PhysRevA.92.023821 PACS number(s): 42.65.Tg, 42.65.Jx, 05.45.Yv, 11.30.Er

I. INTRODUCTION

A common practical requirement for a nonlinear system to have localized solutions is the stability of the zero background. This requirement on the one hand ensures the absence of growing small fluctuations far from the nonlinear mode. More important, this means the stable existence of a system itself without any excitations, i.e., in the "vacuum state," in which the system is prepared experimentally and against which nonlinear modes are excited. In the conservative case this implies the possibility for stable propagation of linear waves (real eigenvalues of the linear Hamiltonian), while in dissipative systems this means decay of all small-amplitude excitations (the background is an attractor with a nonzero basin). In this context parity-time ($\mathcal{PT}$)-symmetric [1,2] systems represent a special case which on the one hand obey gains and losses and on the other hand may have pure real spectra in some domains of the parameter spaces [2] (this situation is referred to as an unbroken $\mathcal{PT}$-symmetric phase [1]) allowing for propagation of linear waves and possessing continuous families of solutions. Therefore, linear potentials like the parabolic [3], Scarff II [4], or $\mathcal{PT}$-symmetric extension of the Rosen-Morse II potential [5] obeying pure real spectra and supporting localized modes received particular attention also from the point of view of the existence of nonlinear families; see Refs. [6–8] and [9], respectively.

Nonlinear modes can also be found in a region where the linear $\mathcal{PT}$ symmetry is broken [7]. Moreover, families of nonlinear modes can be stable [10,11] in those regions. However, the mathematical existence of such nonlinear modes, and even of stable ones, does not yet guarantee their practical utility, because the manner of their excitation in a system that is linearly unstable in its "vacuum" state remains questionable. This leads us to the first goal of the present paper, which is a suggestion on how stable nonlinear modes can be excited in systems where the linear $\mathcal{PT}$ symmetry is broken. The idea is based on the possibility of "switching on" nonlinearity simultaneously with gain and dissipation. Such a possibility can be implemented, in particular, when the nonlinearity and gain-and-loss strength are characterized by a single parameter (let us call it ϵ) and disappear when this parameter becomes zero ($\epsilon = 0$). If at $\epsilon = 0$ the system is Hamiltonian, it allows for stable propagation of the linear modes, and the only stability issue which has to be verified is the stability of the solution branch $\epsilon > 0$, bifurcating from $\epsilon = 0$. Then, if the stability is confirmed, one can consider the adiabatic growth of $\epsilon = \epsilon(t)$ in time as a way to excite a nonlinear mode, which persists in a stable fashion even if the final value of ϵ corresponds to the underlying linear system with a broken $\mathcal{PT}$-symmetric phase.

To solve this problem mathematically, a suitable framework is the use of potentials supporting some exact solutions. Such complex potentials can be constructed, say, using "inverse engineering" as suggested in Ref. [12] (here we also mention other examples of particular exact solutions for $\mathcal{PT}$-symmetric potentials published in Refs. [7,13]). The method consists in computing a complex potential starting with an *a priori* given solution which, however, must satisfy some constraints to ensure the existence of the potential. Generally speaking, the potentials supporting particular exact solutions appear in rather sophisticated forms, which may constitute a significant difficulty for their practical implementation. Therefore, as a complementary task of this paper we consider the generation of the modes in potentials of relatively simple and experimentally feasible forms, bearing in mind their applications in optics of atomic gases [14] as well as in the $\mathcal{PT}$-symmetric physics of Bose-Einstein condensates [15–17], where $\mathcal{PT}$-symmetric potentials can be created and modified *in situ*.

The rest of the paper is organized as follows. In Sec. II, we describe the general theory and approach to the nonlinear Schrödinger equation with the $\mathcal{PT}$-symmetric potentials allowing for exact particular solutions. In Sec. III we discuss applications of the method to the parabolic potential and in Secs. IV and V we consider linear and nonlinear modes in both single-well and double-well potentials, respectively. In particular, the problem of the nonlinear mode excitations in the single-well and double-well $\mathcal{PT}$-symmetric potentials allowing for particular exact solutions is also addressed in Secs. IV and V. Our results are summarized in the Conclusion.

*zyyan@mmrc.iss.ac.cn

II. GENERAL THEORY AND APPROACH

We consider the nonlinear Schrödinger (NLS) equation with the $\mathcal{PT}$-symmetric potential and space-modulated nonlinearity (abbreviated below as $\mathcal{PT}$-NLSE)

$$i\partial_t\psi = -\tfrac{1}{2}\partial_x^2\psi + U_\epsilon(x)\psi + G_\epsilon(x)|\psi|^2\psi, \tag{1}$$

where $\partial_t = \partial/\partial t$, $\partial_x = \partial/\partial x$, $\psi = \psi(x,t)$ is the complex envelope of the electrical field, $U_\epsilon(x) = U_\epsilon^*(-x)$ (i.e., $\mathrm{Re}[U_\epsilon(x)] = \mathrm{Re}[U_\epsilon(-x)]$, $\mathrm{Im}[U_\epsilon(x)] = -\mathrm{Im}[U_\epsilon(-x)]$) and $G_\epsilon(x)$ describe the complex-valued linear $\mathcal{PT}$-symmetric potential and real-valued inhomogeneous nonlinearity, respectively, and an asterisk stands for complex conjugation. For specific real-valued potential, i.e., if $U_\epsilon(x) = U_\epsilon^*(x)$, Eq. (1) reduces to the conservative NLS equation with space-modulated linear and nonlinear coefficients. In that case, particular exact solutions and corresponding dynamical behaviors were extensively studied in the literature (see, e.g., Refs. [18–22]).

In order to implement the procedure described in the Introduction we assume that

$$U_\epsilon(x) = \sum_{j=0}^{2}\epsilon^{2j}V_j(x) + i\epsilon W(x), \tag{2}$$

$$G_\epsilon(x) = \epsilon^2 G(x), \tag{3}$$

where $V_j(x)$ $(j = 0,1,2)$ are constituents of the real potential, $W(x)$ is the real gain-and-loss distribution, and $\epsilon \geqslant 0$ is the bifurcation parameter parametrizing a branch of the solutions; we emphasize that generally speaking ϵ is not considered small. To ensure the $\mathcal{PT}$ symmetry we consider $V_j(x) = V_j(-x)$ $(j = 0,1,2)$ and $W(x) = -W(-x)$. At $\epsilon = 0$, Eq. (1) becomes the linear Schrödinger equation. Our main interest focuses on the case where $W(x) \not\equiv 0$ (i.e., when the linear potential $U_\epsilon(x)$ is non-Hermitian).

We concentrate on stationary solutions of $\mathcal{PT}$-NLSE (1) in the form $\psi(x,t) = \phi(x)e^{-i\mu t}$, where μ is a real spectral parameter, and the complex-valued nonlinear eigenmode $\phi(x)$ satisfies the stationary NLS equation

$$\mu\phi = -\frac{1}{2}\frac{d^2\phi}{dx^2} + U_\epsilon(x)\phi + G_\epsilon(x)|\phi|^2\phi, \tag{4}$$

subject to the zero boundary conditions $\lim_{x\to\pm\infty}\phi(x) = 0$.

Now, following the strategy described in the Introduction we assume that the solution of the linear eigenvalue problem

$$L_0\tilde{\phi}_n(x) = \tilde{\mu}_n\tilde{\phi}_n(x), \quad L_0 = -\frac{1}{2}\frac{d^2}{dx^2} + V_0(x), \tag{5}$$

where $n = 0,1,2,\ldots,$ is known. In Eq. (5) we assume also that the spectrum is discrete (which is applied for all examples considered in this paper) and distinguish the eigenfunctions and eigenvalues of this linear problem by tildes. In order to obtain a nonlinear branch of solutions ϕ_n which bifurcates from $\tilde{\phi}_n(x)$ we require $\lim_{x\to\pm\infty}\tilde{\phi}_n(x) = 0$. Thus, all $\tilde{\phi}_n(x)$ can be considered real without loss of generality. Since L_0 is Hermitian, all the eigenvalues $\tilde{\mu}_n$ are also real, which indicates the stability of the respective linear system (here we exclude the situation where zero is an eigenvalue of L_0).

Turning now to $\epsilon > 0$ we observe that in the presence of gain-and-loss distribution, stationary modes (if any) must have nonzero (hydrodynamic) current, i.e., an x-dependent argument. Respectively we consider the construction of the $\mathcal{PT}$-symmetric potential and nonlinearity for modes having the form

$$\phi_n(x) = \tilde{\phi}_n(x,\epsilon)\exp\left(i\epsilon\int_{-\infty}^{x}v_n(\xi)d\xi\right), \tag{6}$$

where the real function $v_n(x)$ is the hydrodynamic velocity and n stands here for the identification of the family bifurcating from the nth linear eigenstate. Since this ansatz implies that the modulus of the nonlinear modes persists equal to the linear distribution, the possibility of constructing such modes is not obvious. In order to address this issue we substitute Eq. (6) in Eq. (4) and obtain relations linking the phase,

$$\frac{d}{dx}(v_n(x)|\tilde{\phi}_n(x,\epsilon)|^2) = 2W(x)|\tilde{\phi}_n(x,\epsilon)|^2, \tag{7}$$

and the amplitude,

$$\tfrac{1}{2}v_n^2(x) + G(x)|\tilde{\phi}_n(x,\epsilon)|^2 + V_1(x) + \epsilon^2 V_2(x) = \nu_n, \tag{8}$$

where we introduce the shift of the eigenvalue ν_n determined by $\mu - \tilde{\mu}_n = \epsilon^2\nu_n$.

The last equation has a free parameter ϵ which leaves much freedom in constructing a solution. Although we do not require ϵ to be small, we nevertheless restrict further consideration to two basic cases as follows:

Case 1. The amplitude of $\phi_n(x)$ is independent on ϵ, i.e., $\tilde{\phi}_n(x,\epsilon) = \tilde{\phi}_n(x)$ and

$$\tfrac{1}{2}v_n^2(x) + G(x)\tilde{\phi}_n^2(x) + V_1(x) = \nu_n, \quad V_2(x) \equiv 0. \tag{9}$$

Case 2. The amplitude of $\phi_n(x)$ is proportional to ϵ, i.e., $\tilde{\phi}_n(x,\epsilon) = \epsilon\tilde{\phi}_n(x)$ and

$$\tfrac{1}{2}v_n^2(x) + V_1(x) = \nu_n, \quad G(x)\tilde{\phi}_n^2(x) + V_2(x) = 0. \tag{10}$$

The obtained system (7) with Eq. (8) [cf. Eq. (9) or Eq. (10)] still contains freedom in the definition of the potentials and the hydrodynamic velocity. Therefore, we impose further constraints on the linear part $V_j(x)$ for $j \geqslant 1$, $W(x)$ and nonlinear $G(x)$ potentials, as well as the hydrodynamic velocity $v_n(x)$, requiring them to be localized, i.e., $V_j(x) \to 0$ for $j \geqslant 1$, $W(x) \to 0$, $G(x) \to 0$, and $v_n(x) \to 0$ at $|x| \to \infty$. Considering now Eq. (8) in the limit $|x| \to \infty$ we readily obtain that $\nu_n = 0$. Thus, in this case a nonlinear mode has not only the same form but also the same eigenvalue as its linear counterpart at $\epsilon = 0$ does.

Thus, we have obtained the profiles of the nonlinear modes in an exact analytical form $\psi_n(x,t) = \phi_n(x)e^{-i\mu_n t}$ with $\phi_n(x)$ being given by Eq. (6). Our next main task is to study the stability of the nonlinear modes. We do this numerically by two standard approaches. First, we address the linear stability of a nonlinear mode $\psi_n(x,t) = \phi_n(x)e^{-i\mu_n t}$, employing the ansatz

$$\psi_n(x,t) = \{\phi_n(x) + \varrho[f(x)e^{-i\delta t} + g^*(x)e^{i\delta^* t}]\}e^{-i\mu_n t}, \tag{11}$$

where $\varrho \ll 1$, and $f(x)$ and $g(x)$ are the eigenfunctions of the linear eigenvalue problem:

$$\begin{pmatrix} L_\epsilon & G_\epsilon(x)\phi_n^2(x) \\ -G_\epsilon(x)\phi_n^{*2}(x) & -L_\epsilon^* \end{pmatrix}\begin{pmatrix} f \\ g \end{pmatrix} = \delta\begin{pmatrix} f \\ g \end{pmatrix} \tag{12}$$

with

$$L_\epsilon = -\tfrac{1}{2}\partial_x^2 + U_\epsilon(x) + 2G_\epsilon(x)|\phi_n(x)|^2 - \mu_n. \quad (13)$$

The solution is linearly unstable if δ has a nonzero imaginary part; otherwise it is stable.

Second, we test the stability by direct propagation using an exact solution $\psi_n(x,t) = \phi_n(x)e^{-i\mu_n t}$ with $\phi_n(x)$ given by Eq. (6) with a noise perturbation of order 1% of the initial amplitude $|\psi_n(x,0)|$, as the initial condition for Eq. (1).

III. PERTURBED $\mathcal{PT}$-SYMMETRIC LINEAR PARABOLIC POTENTIAL

Below we concentrate on the physically relevant case of the parabolic (harmonic) potential $V_0(x) = \omega^2 x^2/2$. Without loss of generality, one can scale out the frequency ω, making it 1, to yield

$$V_0(x) = \tfrac{1}{2}x^2. \quad (14)$$

The families of the nonlinear modes of this potential at $W(x) = x$, $V_j(x) \equiv 0$ $(j = 1,2)$ and constant nonlinearity $G(x) \equiv$ const were considered in Ref. [6].

Now the profile of linear modes related to Eq. (5) is described by the Gauss-Hermite functions

$$\tilde{\phi}_n(x) = H_n(x)e^{-x^2/2}, \quad (15)$$

where $H_n(x) = (-1)^n e^{x^2}(d^n e^{-x^2})/(dx^n)$ is the Hermite polynomial with $n = 0,1,2,\ldots$, and the eigenvalue is

$$\mu = \tilde{\mu}_n = n + \tfrac{1}{2}, \quad (16)$$

in which we have $v_n = 0$.

We also concentrate on the specific Gaussian form of the nonlinearity

$$G(x) = 2\sigma e^{-\alpha x^2} \quad (17)$$

with the characteristic width $1/\sqrt{\alpha}$ with $\alpha > 0$ and constant σ (in particular, the nonlinearity is a constant for $\alpha = 0$). This is a natural choice, for example, for the Bose-Einstein applications, where nonlinearity can be controlled through the optical Feshbach resonance, with $G(x)$ describing the profile of the laser beam (see, e.g., Ref. [23]).

Thus, the solution of the problem is reduced to two steps as follows. First, given the gain-and-loss distribution $W(x)$ from Eq. (7) one obtains the hydrodynamic velocity:

$$v_n(x) = \frac{2}{|\tilde{\phi}_n(x,\epsilon)|^2}\int_{-\infty}^{x} W(\xi)|\tilde{\phi}_n(\xi,\epsilon)|^2 d\xi. \quad (18)$$

Second, the "correction" to the conservative part of the Hamiltonian is computed from Eqs. (9) and (10), with $G(x)$, $v_n(x)$, and $\tilde{\phi}_n(x)$ given by Eqs. (17), (18), and (15).

In the meantime, formula (18) imposes the additional constraint on the choice of the imaginary potential $W(x)$, which must ensure the existence of the integral in Eq. (18). This problem can be overcome if one again uses inverse engineering, i.e., considers the hydrodynamic velocity given and finds $W(x)$ from Eq. (7).

IV. A SINGLE-WELL POTENTIAL

A. $\mathcal{PT}$-symmetry phases of the linear problem

The simplest single-well potential is obtained by setting $V_j(x) \equiv 0$ $(j = 1,2)$, which corresponds to case 1 in Eq. (9) [in case 2 in Eq. (10) one has $G(x)\tilde{\phi}_n^2(x) \equiv 0$, which is the trivial solution]. Recalling that $\tilde{\mu}_n$ is given by Eq. (16) (i.e., $v_n = 0$) and considering $\tilde{\phi}_n(x)$ given by Eq. (15) we readily conclude that such a choice is possible only for attractive (focusing) nonlinearities $\sigma < 0$ (without loss of generality we set $\sigma = -1$) for which the hydrodynamic velocity reads

$$v_n(x) = 2H_n(x)e^{-(\alpha+1)x^2/2}. \quad (19)$$

Now from Eq. (7) we can find the gain-and-loss distributions (i.e., the imaginary part of the potential)

$$W_n(x) = [6nH_{n-1}(x) - (\alpha+3)xH_n(x)]e^{-(\alpha+1)x^2/2}. \quad (20)$$

In order for $W_n(x)$ to be an odd function, i.e., to support $\mathcal{PT}$ symmetry, we require n to be an even number: $n = 0,2,4,\ldots$. The functions $W_n(x)$ with odd n are even and do not satisfy the condition of $\mathcal{PT}$ symmetry. We do not consider them here but observe that for odd n Eq. (4) still obeys exactly localized solutions of the form (6) with $V_0(x)$, $\tilde{\phi}_n(x)$, $G(x)$, $v_n(x)$, and $W_n(x)$ given by Eqs. (14), (15), (17), (19), and (20), respectively.

We also observe that all the members of the $W_n(x)$ family of potentials (i.e., the potentials corresponding to different n) are *two*-parametric, i.e., they are determined by the amplitude [it is given by ϵ when substituted in $U_\epsilon(x)$] and by the internal parameter α.

In order to establish domains of the unbroken $\mathcal{PT}$-symmetry phase of the linear $\mathcal{PT}$-symmetric potential U_ϵ for different n we address the spectral problem

$$\hat{L}_n\Psi(x) = \lambda_n\Psi(x), \quad \hat{L}_n = L_0 + i\epsilon W_n(x), \quad (21)$$

where L_0 is given by Eq. (5), and λ_n and $\Psi(x)$ are eigenvalues and eigenfunctions, respectively. Since the discrete spectrum of a $\mathcal{PT}$-symmetric potential is either real or appears in complex conjugated pairs, we conclude there exists a nonzero domain of the parameter ϵ for which the $\mathcal{PT}$ symmetry remains unbroken.

The simplest potentials with nonzero complex parts are given by $n = 0$,

$$U_\epsilon(x) = \frac{x^2}{2} - i\epsilon(\alpha+3)xe^{-(\alpha+1)x^2/2}, \quad (22)$$

and $n = 2$,

$$U_\epsilon(x) = \frac{x^2}{2} - 2i\epsilon x[2(\alpha+3)x^2 - (\alpha+15)]e^{-(\alpha+1)x^2/2}. \quad (23)$$

In Fig. 1 we show the domains of broken and unbroken phases on the (α,ϵ) plane. Both curves in the figure grow with α, which can be understood from the fact that the growth of α corresponds to the shrinking of the gain-and-loss domains.

In both cases, illustrated in Fig. 2, spontaneous symmetry breaking occurs due to collision of the two lowest states as α decreases (which corresponds to the increase of the width of the gain-and-loss domains). All upper eigenstates (we checked numerically for the six lowest states) remain real. This can be understood from the fact that for the levels with large n the

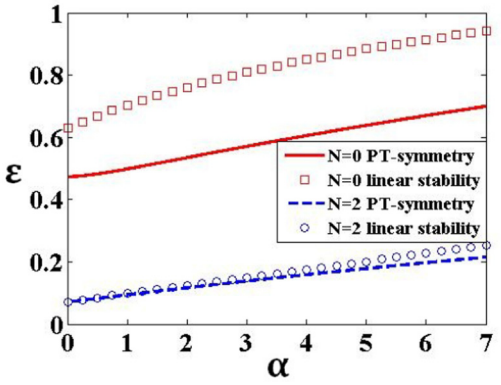

FIG. 1. (Color online) Solid (red) and dashed (blue) curves indicate the lines of phase transitions for the $\mathcal{PT}$-symmetric potentials (22) and (23) with $n = 0, 2$. The unbroken (broken) $\mathcal{PT}$-symmetric phase is in the domain below (above) the phase-breaking lines. Squares (red) and circles (blue) indicate the lines of linear stability of solitons (24) with $n = 0, 2$. The stable (unstable) soliton is in the domain below (above) the linear stable lines.

imaginary part of the potential represents a weak perturbation while the lowest levels are the most strongly deformed ones. We also notice that the instability is oscillatory (i.e., the two emergent complex eigenvalues have a nonzero real part).

B. Nonlinear modes in a single-well potential

Now we turn to the nonlinear modes in the $\mathcal{PT}$-symmetric potentials (22) and (23). The expression for the nonlinear modes is obtained from Eqs. (6) and (19):

$$\phi_n(x) = H_n(x)e^{-x^2/2}\exp\left(2i\epsilon\int_{-\infty}^{x} H_n(\xi)e^{-(\alpha+1)\xi^2/2}d\xi\right). \tag{24}$$

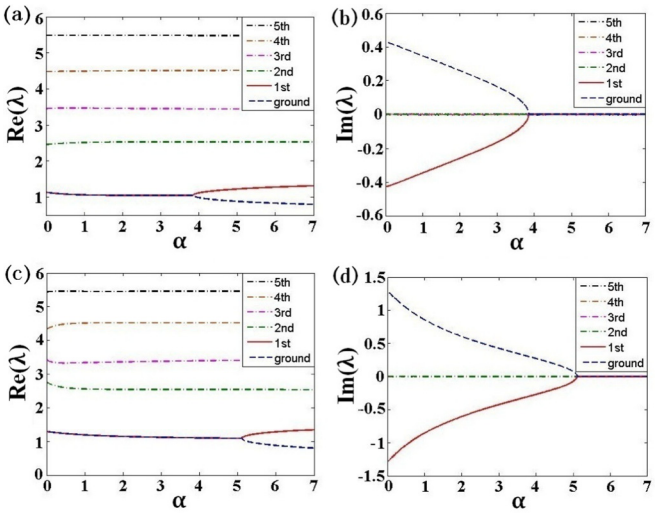

FIG. 2. (Color online) (a, c) Real and (b, d) imaginary parts of the eigenvalues λ_n [see Eq. (21)] as functions of α for the potential (22) at $n = 0, \epsilon = 0.6$ (top row) and for the potential (23) at $n = 2, \epsilon = 0.18$ (bottom row).

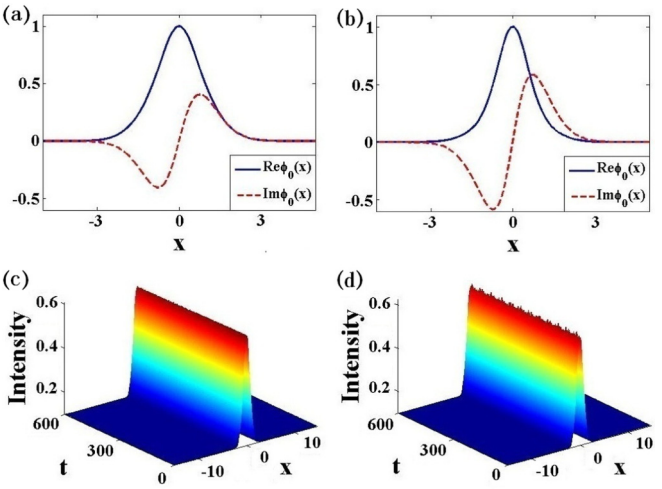

FIG. 3. (Color online) One-hump nonlinear modes given by Eq. (24) with $n = 0$ and $\alpha = 1$ for (a) $\epsilon = 0.45$ (real spectrum of the operator $\hat{L}_0$, i.e., unbroken linear $\mathcal{PT}$ symmetry) and (b) $\epsilon = 0.7$ (broken linear $\mathcal{PT}$ symmetry). (c) Stable and (d) periodically varying propagation of the nonlinear modes described by Eq. (24) and corresponding to the weakly perturbed initial conditions shown in (a) and (b), respectively.

Two examples of the modes are illustrated in Fig. 3 and their linear stability analysis is presented Fig. 1. The feature most relevant to the present consideration is displayed by the domains between the solid line and squares for $n = 0$ and between the dashed line and circles for $n = 2$. In these domains the nonlinear modes [given by Eq. (24) with $n = 0$ and $n = 2$] are stable, while the respective linear $\mathcal{PT}$-symmetric phases are broken; i.e., the linear stability of the nonlinear modes is extended beyond the unbroken linear $\mathcal{PT}$-symmetric phase. Below we explore these domains in order to "draw" the mode along the branch bifurcating from the linearly stable mode. Before that, however, we show the check of stability by means of the direct propagation of the initially stationary state in Eq. (24) with a noise perturbation of order 1%. In Fig. 3(c) we show stable propagation of the soliton for the parameters belonging to the domain of the unbroken linear $\mathcal{PT}$-symmetric phase of the operator $\hat{L}_0$ [defined in Eq. (21)] and to the linearly stable nonlinear mode. In Fig. 3(d) we illustrate the evolution of the mode where the linear $\mathcal{PT}$-symmetric phase is broken and the nonlinear mode is linearly stable. In this last case we observe the oscillatory (breather-like behavior).

Similarly, Figs. 4(a) and 4(c) display the initial states and stable intensity evolution of a two-hump solitary wave [described by Eq. (24) with $n = 2$] for the parameters which guarantee both the real spectrum of the operator $\hat{L}_2$ (unbroken $\mathcal{PT}$-symmetric phase) as well as the linear stability of the nonlinear mode. In the meantime, Figs. 4(b) and 4(d) show a two-hump soliton for the parameters corresponding to broken linear $\mathcal{PT}$ symmetry but still stable in the nonlinear mode. In both numerical simulations we observed robustness of the nonlinear modes with respect to weak initial noise.

Now we turn to the excitation of nonlinear modes by means of a slow change of the control parameter $\epsilon(t)$ which is now considered as a function of time. More specifically we

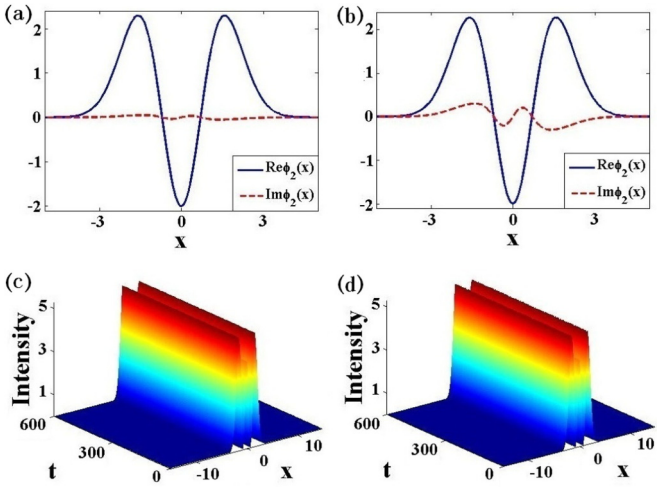

FIG. 4. (Color online) Two-hump nonlinear modes given by Eq. (24) with $n = 2$ and $\alpha = 2$ for (a) $\epsilon = 0.02$ (real spectrum of the operator $\hat{L}_2$, i.e., unbroken linear $\mathcal{PT}$ symmetry) and (b) $\epsilon = 0.12$ (broken linear $\mathcal{PT}$ symmetry). Both nonlinear modes are linearly stable (see Fig. 1), which is illustrated in (c) and (d) where the direct numerical simulations of Eq. (24) are performed with weakly perturbed initial profiles (a) and (b).

consider simultaneous adiabatic switching on the gain-and-loss distribution and the nonlinearity, modeled by [cf. Eq. (1)]

$$i\partial_t\psi = -\tfrac{1}{2}\partial_x^2\psi + [V_0(x) + i\epsilon(t)W_n(x)]\psi + \epsilon^2(t)G(x)|\psi|^2\psi, \tag{25}$$

where the single-well potential $V(x)$, nonlinearity $G(x)$, and gain-and-loss distribution $W(x)$ are given by Eqs. (14), (17), and (20), respectively, and

$$\epsilon(t) = \begin{cases} 0.2\sin\left(\frac{\pi t}{1200}\right) + 0.45, & 0 \leqslant t < 600 \\ 0.65, & 600 \leqslant t \leqslant 1200. \end{cases} \tag{26}$$

This choice of the final value of ϵ is justified by the fact that the whole "trajectory" $\epsilon(t)$, shown in Fig. 5(a), belongs to the parameter domain where the nonlinear mode is stable.

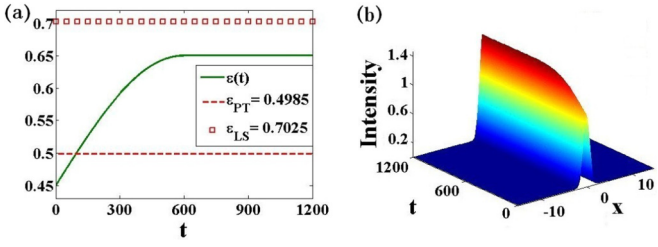

FIG. 5. (Color online) (a) Time dependence of the parameter $\epsilon(t)$ (solid line) given by Eq. (26). The squares and solid line (corresponding to the squares and dashed line in Fig. 1) indicate the $\mathcal{PT}$-symmetry-breaking phase transition in the linear case and loss of the stability of the nonlinear modes, respectively. (b) Intensity evolution of a nonlinear mode governed by Eq. (25) with the initial condition $\psi_0(x,t=0) = \phi_0(x)$ given by Eq. (24) at $\epsilon = 0.45$ for the single-well potential $V_0(x)$ (14) and gain-and-loss distribution $W_0(x)$ (20). Other parameters are $n = 0$ and $\alpha = 1$.

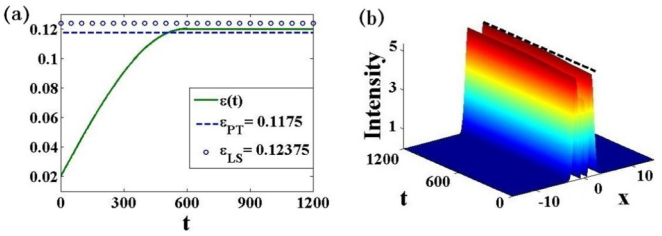

FIG. 6. (Color online) (a) Time dependence of the parameter $\epsilon(t)$ (solid line) given by Eq. (27). The circles and dashed line are explained in Fig. 1. (b) Intensity evolution of a two-hump nonlinear mode of Eq. (25) with $n = 2$, and $\alpha = 2$ subject to the initial condition $\psi_2(x,t=0) = \phi_2(x)$ given by Eq. (24) at $\epsilon = 0.02$ for the single-well potential $V_0(x)$ (14) and gain-and-loss distribution $W_2(x)$ (20). The dashed line shows the finally established amplitude of the mode which is different.

Figure 5(b) exhibits the evolution of the solution $\psi(x,t)$ governed by Eqs. (25) and (26) subject to the initial condition given by Eq. (24) with $n = 0$, i.e., for the single-well potential $V_0(x)$, nonlinearity $G(x)$, and gain-and-loss distribution $W_0(x)$ given by Eqs. (14), (17), and (20), respectively. One observes remarkably stable propagation with the increasing amplitude of nonlinear modes, which is driven from a nonlinear mode at the system parameters of the unbroken linear $\mathcal{PT}$-symmetric phase, to the stable nonlinear mode at the parameters where the linear $\mathcal{PT}$-symmetric phase is broken [i.e., while $\epsilon(t)$ is growing there occurs the linear $\mathcal{PT}$-symmetry phase transition and linear modes become unstable].

Next we consider the excitation of the mode (24) with $n = 2$ described by Eq. (25) with the control parameter adiabatically changing according to the law [see Fig. 6(a)]

$$\epsilon(t) = \begin{cases} 0.1\sin\left(\frac{\pi t}{1200}\right) + 0.02, & 0 \leqslant t < 600, \\ 0.12, & 600 \leqslant t \leqslant 1200. \end{cases} \tag{27}$$

The single-well potential $V_0(x)$, nonlinearity $G(x)$, and gain-and-loss distribution $W_2(x)$ are given by Eqs. (14), (17), and (20), respectively.

Like in the previous case we observe a stable evolution of the nonlinear mode "prepared" in a system with an unbroken $\mathcal{PT}$-symmetric phase and drawn to the system with a broken $\mathcal{PT}$-symmetric phase. The amplitude of the nonlinear mode grows with $\epsilon(t)$ and remains unchanged after the control parameter reaches its final value [see Fig. 6(b)].

V. A DOUBLE-WELL POTENTIAL

A. $\mathcal{PT}$-symmetry phases of the linear problem

Now we consider a multiwell potential with $V_1(x)V_2(x) \not\equiv 0$, which corresponds to case 2 in Eq. (10). Recalling that $\tilde{\mu}_n$ is given by Eq. (16) and considering $\tilde{\phi}_n(x)$ given by Eq. (15) we conclude that now the hydrodynamic velocity takes the form

$$v_n(x) = H_n(x)e^{-x^2/2} \tag{28}$$

(i.e., it is now fixed having no free parameters).

From Eqs. (7) and (10) it follows that the gain-and-loss distributions (i.e., imaginary potentials which are odd functions) numbered by an even number n, i.e., ensuring $\mathcal{PT}$ symmetry of the potential, and generated by the velocity

field (28) are given by

$$W_n(x) = \left[3nH_{n-1}(x) - \tfrac{3}{2}xH_n(x)\right]e^{-x^2/2}. \quad (29)$$

The real parts of the respective linear potential read

$$V_{1n}(x) = -\tfrac{1}{2}H_n^2(x)e^{-x^2}, \quad (30)$$

$$V_{2n}(x) = -2\sigma H_n^2(x)e^{-(\alpha+1)x^2}. \quad (31)$$

All the members of the $W_n(x)$ family of potentials are two-parametric; they are determined by the amplitude given by ϵ in $U_\epsilon(x)$, and by the internal parameter α introduced in Eq. (31).

Unlike in case 1 considered in the previous section, for the case of a multiwell potential the parameter σ [see Eqs. (17) and (31)] need not be nonpositive and can acquire positive values; i.e., the nonlinearity can be either attractive or repulsive. Since, however, in this section we are interested in double-well potentials, we concentrate on the "deformation" of the linear potential

$$U_\epsilon(x) = \frac{x^2}{2} + \epsilon^2 V_{10}(x) + \epsilon^4 V_{20}(x) + i\epsilon W_0(x), \quad (32)$$

where

$$V_{10}(x) = -\tfrac{1}{2}e^{-x^2}, \quad V_{20}(x) = -2\sigma e^{-(\alpha+1)x^2}, \quad (33a)$$

$$W_0(x) = -\tfrac{3}{2}xe^{-x^2/2}, \quad (33b)$$

(this corresponds to the chemical potential $\mu = \tilde{\mu}_0 = 1/2$) and we require $\sigma < -1/(4\epsilon^2)$, the latter constraint ensuring the required double-well shape.

Notice that at $\alpha = 0$ the nonlinearity is a constant [see Eq. (17)] while the real part of the potential $U_\epsilon(x)$ preserves a double-well shape. Nonlinear modes in this case were recently reported in Refs. [17,24] (also, nonlinear modes in a slightly different double-well potential with the imaginary part (33b) were investigated in Ref. [25]). When α increases, the amplitude of the potential barrier between the humps decreases.

As above we start by defining the domains of the unbroken and broken $\mathcal{PT}$-symmetric phase of the underlying linear problem with $n = 0$. Respectively, we consider the linear spectral problem [cf. Eq. (21)]

$$\tilde{L}\Psi = \lambda\Psi, \ \tilde{L} = L_0 + \epsilon^2 V_{10}(x) + \epsilon^4 V_{20}(x) + i\epsilon W_0(x), \quad (34)$$

where L_0 is given by Eq. (5), and λ and $\Psi = \Psi(x)$ are the eigenvalue and eigenfunction, respectively. For the present case it is important that the nonlinearity can also be varied in time and its value affects the stability of the mode. Indeed, in Fig. 7(a) we show the domains of broken and unbroken phases at $\epsilon = 0.8$ on the (α,σ) plane. The parametric dependence of the lowest eigenvalues is shown in Figs. 7(b) and 7(c). Like in the case of the one-hump potential we observe that the unbroken phase corresponds to relatively large α and the spontaneous symmetry breaking occurs as α decreases (which corresponds to the increase of the width of the gain-and-loss domains) due to the collision of the two lowest eigenvalues. However, now the broken phase corresponds to a limited interval of α and we observe the reentered unbroken phase as α approaches zero. We also notice that the instability is oscillatory: the emergent complex eigenvalues have a nonzero real part.

B. Nonlinear modes in a double-well potential

Now we turn to the nonlinear modes in the $\mathcal{PT}$-symmetric double-well potential (32), whose explicit expression is obtained from Eqs. (6) and (28):

$$\phi_n(x) = \epsilon H_n(x)e^{-x^2/2}\exp\left(i\epsilon\int_{-\infty}^{x} H_n(\xi)e^{-\xi^2/2}d\xi\right). \quad (35)$$

The results of the linear stability analysis of solution (35) are shown in Fig. 7(a). The feature most relevant for our consideration consists in the domain, now with respect to σ, where the linear $\mathcal{PT}$ symmetry is broken, while the nonlinear mode remains stable (in analogy with the case of the one-well potential).

The stability of the nonlinear mode (35) with $n = 0$ is also confirmed by the direct propagation with the perturbation of the initial profile, as illustrated in Fig. 8. In Fig. 8(b) we show stable propagation of the soliton for the parameters belonging to the domain of the unbroken linear $\mathcal{PT}$-symmetric phase of the operator $\tilde{L}$ [defined in Eq. (34)], and to the linearly stable nonlinear mode. In Fig. 8(c) we illustrate the evolution of the mode where the linear $\mathcal{PT}$-symmetric phase is broken; however, the nonlinear mode is linearly stable.

Now we turn to the excitation of nonlinear modes in the double-well potential. Since the potential $V_{20}(x)$ and nonlinearity $G(x)$ both contain σ, this parameter σ can be exploited for management (i.e., for excitation, in our case) of

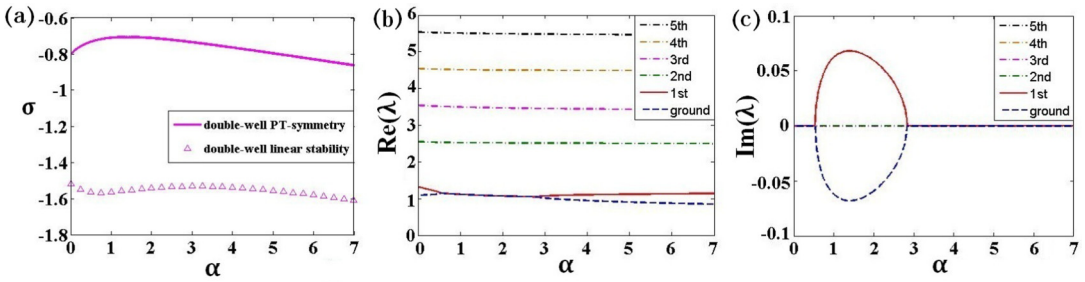

FIG. 7. (Color online) (a) The line of the $\mathcal{PT}$-symmetry phase transition for the $\mathcal{PT}$-symmetric potentials (32). The unbroken (broken) $\mathcal{PT}$-symmetric phase is in the domain above (below) the phase-breaking lines. Triangles indicate the border of the linear stability domain of the mode (35) with $n = 0$. Stable (unstable) solitons are in the domains above (below) the respective border lines. (b) Real and (c) imaginary parts of the eigenvalue λ [see Eq. (34)] as functions of α for the potential (32) at $\sigma = -0.73$. In all panels $\epsilon = 0.8$.

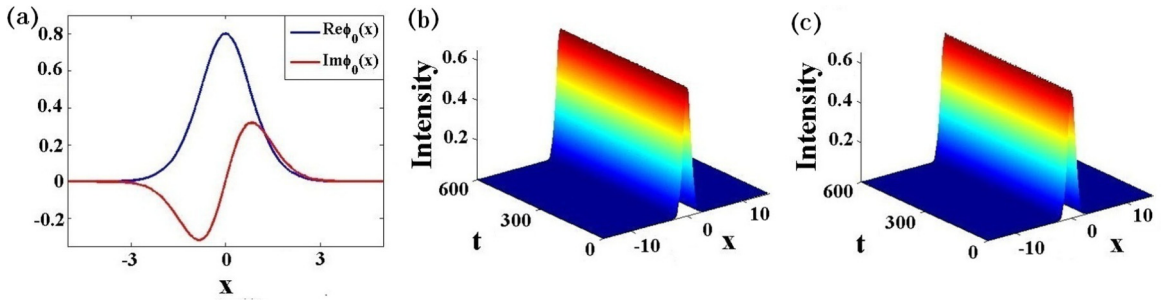

FIG. 8. (Color online) (a) The same nonlinear modes given by Eq. (35) with $n = 0$, $\alpha = 4$, $\epsilon = 0.8$ for both $\sigma = -0.65$ (real spectrum of the operator $\tilde{L}$, i.e., unbroken linear $\mathcal{PT}$ symmetry) and $\sigma = -1.25$ (broken linear $\mathcal{PT}$ symmetry). Both nonlinear modes are linearly stable [see Fig. 7(a)] which are illustrated in (b) and (c) where the direct numerical simulations of Eq. (35) are performed with a weakly perturbed initial profile (a) for different parameters $\sigma = -0.65$ and $\sigma = -1.25$, respectively.

the nonlinear modes. To this end we consider σ to be a function of t and address the adiabatic switch-on of the potential and the nonlinearity, governed by the model (1) which now is rewritten in the form

$$i\partial_t\psi = -\tfrac{1}{2}\partial_x^2\psi + [V_0(x) + \epsilon^2 V_{10}(x) + \epsilon^4 V_{20}(x;\sigma(t)) + i\epsilon W_0(x)]\psi + \epsilon^2 G(x;\sigma(t))|\psi|^2\psi. \quad (36)$$

Here the double-well potential $V_{10}(x)$ and gain-and-loss distribution $W_0(x)$ are given by Eqs. (33a) and (33b), respectively, and $V_{20}(x;\sigma(t))$ and $G(x;\sigma(t))$ stand for $V_{20}(x)$ and $G(x)$ given by Eqs. (33a) and (17) with σ replaced by $\sigma(t)$.

According the general idea described above, now we choose the *adiabatic change* of $\sigma(t)$ in such a way that it ensures that the system evolves from the domain of the unbroken $\mathcal{PT}$ symmetry of the underlying linear model to a broken phase where, however, the nonlinear mode is linearly stable. More specifically, in the numerical simulations we exploit the dependence

$$\sigma(t) = \begin{cases} -0.6\sin\left(\frac{\pi t}{1200}\right) - 0.65, & 0 \leqslant t < 600, \\ -1.25, & 600 \leqslant t \leqslant 1200. \end{cases} \quad (37)$$

The dependence $\sigma(t)$ is illustrated in Fig. 9(a).

Figure 9(b) exhibits the excitation of a nonlinear mode described by Eq. (36) for the double-well potential, i.e., $V_0(x)$, $V_{10}(x)$, $V_{20}(x;\sigma(t))$, nonlinearity $G(x;\sigma(t))$ and gain-and-loss distribution $W_0(x)$ determined by Eq. (37) for the varying parameter $\sigma(t)$. The initial condition in these simulations has taken the form of (35) with $n = 0$. In the figure we again observe the stable evolution of the nonlinear mode between the initial and final shapes of the potential (notice that the change of the mode amplitude is relatively small and not clearly visible on the scale of the figure).

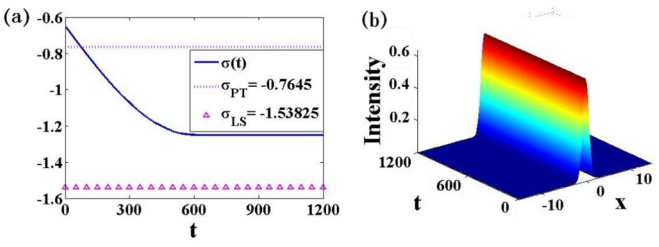

FIG. 9. (Color online) (a) Time dependence of the parameter $\sigma(t)$ given by Eq. (37) (solid line). Dashed line and triangles indicate boundaries of the stability of the nonlinear mode and the unbroken $\mathcal{PT}$-symmetric phase (in both cases above the respective curve). (b) Intensity evolution of the nonlinear mode of Eq. (36) with the initial condition given by Eq. (35) for the double-well potential with $n = 0$, $\alpha = 4$, and $\epsilon = 0.8$.

VI. DISCUSSION AND CONCLUSIONS

In the present paper we reported several new branches of nonlinear modes described by the nonlinear Schrödinger equation with the $\mathcal{PT}$-symmetric single-well and double-well potentials and Hermite-Gaussian distributions of the gains and losses. The reported solutions are two-parametric, each of the parameters defining a branch of the solutions. All the considered branches bifurcate from the modes of the respective linear potentials. A peculiarity of the reported modes consists in their stability properties: their stability in the parameter space extends beyond the domains of the stability of the respective limits, i.e., beyond the domain of the unbroken $\mathcal{PT}$-symmetric phase of the underlying linear problem. This suggests a possibility of how a stable nonlinear mode can be excited in a $\mathcal{PT}$-symmetric system with broken $\mathcal{PT}$ symmetry. The method is based on drawing the mode by adiabatic change of one of the control parameters along the branch from the domain where linear stability is verified and the $\mathcal{PT}$-symmetric phase is unbroken, i.e., where the mode can be excited by one of the conventional methods, to the domain where the $\mathcal{PT}$ symmetry is broken but the nonlinear stability still persists. Notices that when $\mathcal{PT}$ symmetry is broken, the ground and the first excited states are indistinguishable in Figs. 2 and 7.

While the described approach is straightforward mathematically it leaves an open problem on managing gains and losses by a single parameter, while in many cases the physical phenomena responsible for gains and losses have different natures. Speaking more generally, to implement the suggested scheme in practice one need not hold an integrable model but one does need to preserve balance between the gains and losses. This last goal can be achieved in at least one of the following ways. First, considering $\mathcal{PT}$-symmetric profiles created in mixtures of atomic gases [14], one can modify both active and lossy domains by a single parameter, which is the intensity or wavelength of the control field, or alternatively by

varying in space the properties of cladding of the atomic cell. The latter affects the whole spectrum of the underlying linear problem, i.e., both real and imaginary parts of the refractive index. On the other hand, when considering $\mathcal{PT}$-symmetric double-well potentials in Bose-Einstein condensate problems, to ensure the balance between varying gains and losses one has to perform simultaneous loading of atoms to one of the wells (either using an atomic laser [26] or tunneling from a neighbor potential well, as suggested in Ref. [16]) and eliminating atoms (using, for example, ionization by an external beam [27] or leakage of atoms through tunneling [16]).

Finally, returning to the considered exact model, the method was tested using the found exact solutions in the form of one- and two-hump modes supported by the one-well $\mathcal{PT}$-symmetric potential and by the repulsive nonlinearity, as well as for the modes in a double-well potential and attractive nonlinearity. In all the cases we observed the stable evolution of nonlinear modes, thus supporting the practical feasibility of the approach.

ACKNOWLEDGMENTS

Z.Y. and Z.W. were partially supported by the NSFC (Grant No. 61178091) and NKBRPC (Grant No. 2011CB302400). V.V.K. acknowledges support of the FCT (Portugal) Grants No. UID/FIS/00618/2013 and No. PTDC/FIS-OPT/1918/2012.

[1] C. M. Bender and S. Boettcher, Phys. Rev. Lett. **80**, 5243 (1998).
[2] C. M. Bender, Rep. Prog. Phys. **70**, 947 (2007).
[3] T. Kato, *Perturbation Theory for Linear Operators* (Springer-Verlag, Berlin, 1980); M. Znojil, Phys. Lett. A **259**, 220 (1999).
[4] Z. Ahmed, Phys. Lett. A **282**, 343 (2001); **287**, 295 (2001).
[5] G. Lévai and E. Magyari, J. Phys. A: Math. Theor. **42**, 195302 (2009).
[6] D. A. Zezyulin and V. V. Konotop, Phys. Rev. A **85**, 043840 (2012).
[7] Z. H. Musslimani, K. G. Makris, R. El-Ganainy, and D. N. Christodoulides, Phys. Rev. Lett. **100**, 030402 (2008).
[8] H. Chen, S. Hu, and L. Qi, Opt. Commun. **331**, 139 (2014); Z. Shi, X. Jiang, X. Zhu, and H. Li, Phys. Rev. A **84**, 053855 (2011).
[9] B. Midya and R. Roychoudhury, Phys. Rev. A **87**, 045803 (2013).
[10] D. A. Zezyulin and V. V. Konotop, Phys. Rev. Lett. **108**, 213906 (2012).
[11] Y. Lumer, Y. Plotnik, M. C. Rechtsman, and M. Segev, Phys. Rev. Lett. **111**, 263901 (2013).
[12] F. K. Abdullaev, V. V. Konotop, M. Salerno, and A. V. Yulin, Phys. Rev. E **82**, 056606 (2010).
[13] Z. Y. Yan, B. Xiong, and W.-M. Liu, arXiv:1009.4023; Z. Y. Yan, Philos. Trans. R. Soc. A **371**, 20120059 (2013); Z. C. Wen and Z. Y. Yan, Phys. Lett. A **379**, 2025 (2015).
[14] C. Hang, G. Huang, and V. V. Konotop, Phys. Rev. Lett. **110**, 083604 (2013); C. Hang, D. A. Zezyulin, V. V. Konotop, and G. Huang, Opt. Lett. **38**, 4033 (2013); H. Li, J. Dou, and G. Huang, Opt. Express **21**, 312053 (2013); C. Hang, D. A. Zezyulin, G. Huang, V. V. Konotop, and B. A. Malomed, Opt. Lett. **39**, 5387 (2014).
[15] S. Klaiman, U. Günther, and N. Moiseyev, Phys. Rev. Lett. **101**, 080402 (2008); H. Cartarius and G. Wunner, Phys. Rev. A **86**, 013612 (2012).
[16] M. Kreibich, J. Main, H. Cartarius, and G. Wunner, Phys. Rev. A **87**, 051601 (2013).
[17] D. Dast, D. Haag, H. Cartarius, J. Main, and G. Wunner, J. Phys. A: Math. Theor. **46**, 375301 (2013).
[18] J. Belmonte-Beitia, V. M. Perez-Garcia, V. Vekslerchik, and P. J. Torres, Phys. Rev. Lett. **98**, 064102 (2007); V. N. Serkin, A. Hasegawa, and T. L. Belyaeva, *ibid.* **98**, 074102 (2007).
[19] J. Belmonte-Beitia, V. M. Pérez-García, V. Vekslerchik, and V. V. Konotop, Phys. Rev. Lett. **100**, 164102 (2008).
[20] H. Friedrich, G. Jacoby, and C. G. Meister, Phys. Rev. A **65**, 032902 (2002); Yu. V. Bludov, Z. Y. Yan, and V. V. Konotop, *ibid.* **81**, 063610 (2010).
[21] Z. Y. Yan and V. V. Konotop, Phys. Rev. E **80**, 036607 (2009).
[22] Z. Y. Yan and D. M. Jiang, Phys. Rev. E **85**, 056608 (2012); Z. Y. Yan, Stud. Appl. Math. **132**, 266 (2014).
[23] L. Pitaevskii and S. Stringari, *Bose-Einstein Condensation* (Oxford University Press, Oxford, 2003); C. J. Pethick and H. Smith, *Bose-Einstein Condensation in Dilute Gases*, 2nd ed. (Cambridge University Press, Cambridge, 2008); Y. Kartashov, B. A. Malomed, and L. Torner, Rev. Mod. Phys. **83**, 247 (2011).
[24] B. Midya, Nonlinear Dyn. **79**, 409 (2014).
[25] A. S. Rodrigues, K. Li, V. Achilleos, P. G. Kevrekidis, D. J. Frantzeskakis, and C. M. Bender, Rom. Rep. Phys. **65**, 5 (2013).
[26] N. P. Robins, P. A. Altin, J. E. Debs, and J. D. Close, Phys. Rep. **529**, 265 (2013).
[27] G. Barontini, R. Labouvie, F. Stubenrauch, A. Vogler, V. Guarrera, and H. Ott, Phys. Rev. Lett. **110**, 035302 (2013).